AD-A096 752 SOUTHERN UNIV BATON ROUGE LA DEPT OF MECHANICAL ENGI--ETC F/G 11/6
AN INVESTIGATION OF MECHANISMS EFFECTING ENVIRONMENTAL STRESS C--ETC(U)
APR 80 I J GRAHAM N00019-79-C-0137

UNCLASSIFIED NL

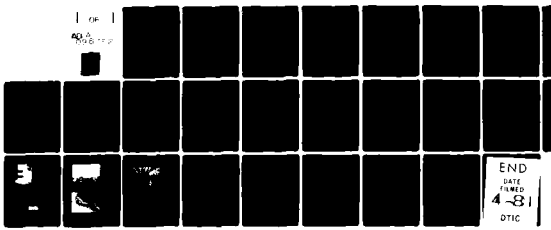

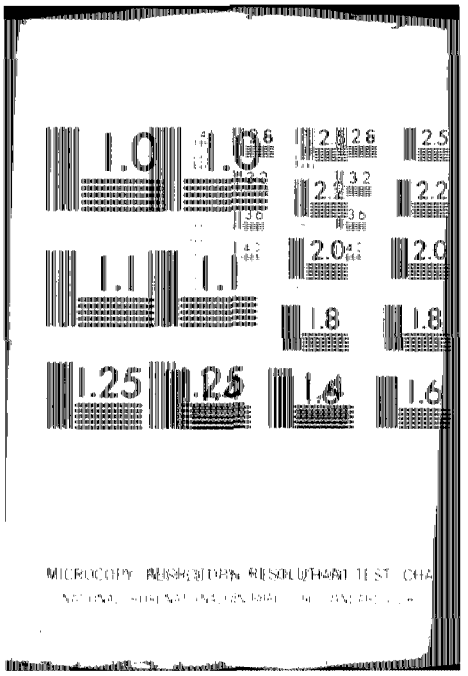
1.0
1.1
1.25
1.8
2.0
2.2
2.5
1.6
MICROCOPY RESOLUTION TEST CHA

(12)

B S

"AN INVESTIGATION OF MECHANISMS EFFECTING ENVIRONMENTAL STRESS CRACKING IN TITANIUM ALLOY"

April 3, 1980

Work Performed Under the Direction of
Ira J. Graham
(Principal Investigator)

Mechanical Engineering Department
Southern University
Baton Rouge, Louisiana 70813

Contract No. N00019-79-C-0137
Naval Air Systems Command
Department of the Navy
Washington, D. C. 20301

Superseded
AD-A086979 (Incomplete)
MC

X

AN INVESTIGATION OF MECHANISMS EFFECTING ENVIRONMENTAL STRESS CRACKING IN TITANIUM ALLOYS

April 3, 1980

Work Performed Under the Direction of
Ira J. Graham
(Principal Investigator)

Mechanical Engineering Department
Southern University
Baton Rouge, Louisiana 70813

Contract No. N00019-79-C-0137
Naval Air Systems Command
Department of the Navy
Washington, D. C. 20301

Acknowledgement

The investigation period involved the efforts of four upper level Mechanical Engineering students, one Civil Engineering student, two junior level Business Management students, the faculty alternate and myself. The writer wishes to express appreciation and thanks for the interest and effort given by Miss. Zenovia Simmons, Rebecca Perry, Valeria Odell and Messers Alaric Buckner and John B. Igbinosum. Also thanks goes to Dr. John Tabony for his assistance as the faculty alternate on the project.

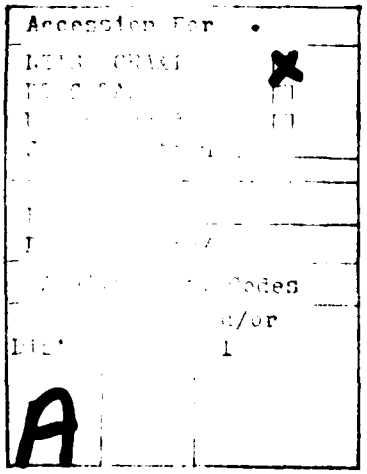

Table of Contents

"An Investigation of Mechanisms of
Environmental Stress Cracking in Titanium Alloy"

Abstract

The acoustic emission technique was applied to monitor visible crack growth and microcrack formations as energy release in real time in titanium alloy using a 12.8 mm (0.510 in) WOL compact specimen in a plane strain mode. The specimens were fatigued in the 30 - 60 Hz range at a determined stress intensity factor (K_1) with an acoustic emission transducer at a gain of 85 dB and a bandpass frequency of 0.1 - 0.3 MHz.

A stable crack advanced and microcracks formed at angles other than parrallel to the advancing stable crack as intermittent energy bursts in or along the boundaries of the grains. The energy release, referred to as "acoustic emission", is a kind of elastic stress impulse. Crack movement in the order of magnitude 10^{-6} in/cyl were detected.

Determination was made of the subcritical stress intensity factor (K_{sc}) where the amplitude of the fatigue cycles no longer provide the energy source large enough to cause the crack to advance.

Introduction

The growth of cracks at subcritical stress intensity levels are responsible for a large percentage of the structural failures encountered in service environments.

The mechanisms that affect the environmental attack are not very well understood. The Acoustic Emission (AE) technology provides a method of detecting crack growth that is not optically visible and of a very small size under various environments and also deriving information that can be related quantitatively. Some data is given in the Tables.

This experimental investigation utilizes the acoustic emission technique to derive information related to the mechanisms that affect the crack advancement and microcrack formation under certain environments on titanium alloy (Ti6Al4V). The acoustic emission is detected through a piezoelectric transducer fitted to the face of a 12.8 mm (0.510in) WOL compact test specimen with a viscous resin and held by a spring. The specimen was given a compliance load and amplitude, and fatigued in the 30 -60 Hz range under load and strain control in the servo-hydraulic electronic closed-loop dynamic test machine.

The electrical output signal from the transducer, which was caused by the stress impulse within the test specimen, is amplified at a gain of 40 dB, and filtered in a frequency bandpass of 0.1 - 0.3 MHz, then amplified again at a gain of 45 dB, hence a total gain of 85 dB. A digital counter in the totalizer counts the newly amplified and filtered signals that exceed one volt peak. The digital-analog converter provides a d-c signal to the X-Y plotter and the emission data is recorded as the test proceeds.

A voltage control gate (VCG) makes it possible to record only signals between the minimum and peak volts, Figure 4. The energy release is also seen as burst type output signals which are controlled by the reset clock. The acoustic signals are counted and held in memory over selected periods of 1 to 2 seconds and printed as linear output signals. The acoustic emission system was able to detect very small crack formation in the order of magnitude 10^{-6} inch/cycle that were not visible through the 32X traveling microscope. The emission counts per cycle per crack extention should provide an area of information for quantitatively relating emission counts to crack growth for an environment relation.

Experimental procedure

A Model 1230 Instron 22 Kip closed-loop servo-hydraulic electronic dynamic test machine was used to load the 12.8 mm (0.510 in) heat treated WOL compact test specimens to the compliance loads shown in Table 1. Six of the test specimens, as seen in Figure 15, were accurately machined in the Mechanical Engineering laboratory and solution heat treated in a Pacific Dual 2800 furnace (electric) which was dried out over an eleven hour period, and then purged with a dry grade nitrogen gas (99.9%) at 5 cubic feet per hour for two hours. The specimens were heated at a rate of 149 C (300 F) per hour and held at 960 C (1760 F) for two hours, then rapidly quenched in oil to room temperature 22 C(74 F). The furnace temperature was cooled down to 734 C (1350 F) and the specimens were replaced in the furnace and held at this

temperature for one hour, then furnace cooled to 560 C (1040 F) at 121 C (250 F) per hour and removed to air cool in the laboratory atmosphere 22 C (74 F) and 62 % humidity.

The specimens developed a thin titanium oxide film which averaged 0.0009 inches thick. The oxide film was removed by light grinding on a surface grinder at 0.0005 inch per pass over the surface, followed by wet belt grinding on 80 and 120 grits silicon carbide abrasive.

The compliance load (ΔK) is given by the equation $\Delta K = B(\sqrt{W})/f(a/w)$. The average stress intensity (ΔK), the difference between $K_{max} - K_q$, was determined by the secant method presented in ASTM-E399 - 75 section 9. The ratio of the maximum load (P_{max}) required to fracture the tensile test specimen and the minimum load (P_q) measured by the secant method was 1.05, which was well below the ratio required to validate the stress intensity factor (K_q) which was determined by the equation: $K_q = P_q/(B)\sqrt{W}\,[29.6(a/w)^{1/2} - 185.5(a/w)^{3/2} + 655.7(a/w)^{5/2} - 1017.0(a/w)^{7/2} + 638.9(a/w)^{9/2}]^2$. The MTS clip gage was set in a fixed gage at zero strain to correlate with zero load and to control the fatigue test in load mode for specimens 3 and 4, while specimen 5 was controlled in the strain mode. The piezoelectric transducer (S140) was attached to the face of each specimen with a viscous resin during the fatigue cycle period. A (801P) preamplifier at 40 dB gain receives the signals and these are filtered in a bandpass frequency of 0.1 - 0.3 MHz and amplified to

a gain of 85 dB in the totalizer. This system is shown in a block diagram, Figure 14. The WOL test specimen was given a tension pre-load of approximately two-thirds the calculated compliance load. This technique reduced and ellimi-nated the pin noise. The load was removed and an initial tension set load was put on the specimen to maintain a tension to tension load mode during the fatigue cycles. The compliance load (ΔP), Table 1, was added to the set load and the instrumentation was calibrated and the stress cracking fatigue cycle started. The traveling microscope was set up to optically follow and measure the crack growth rate while the acoustic signals were recorded as digital output at the X-Y plotter. The acoustic signals were recorded under the voltage control gate (VCG) which was set such that only those signals given off between the selected volt levels were recorded, Table 2. The continuous recording mode was under the control of the reset clock by which the crack emissions were counted, accumulated and recorded at the reset clock interval. The specimen was statically stressed to fracture and the fractured surface was examined under the microscope and macroscopic photographs were made, Figure 6.

The specimen was oriented and sliced on a wet cut-off abrasive wheel. These were mounted in lucite and microstructures were prepared. A Kroll reagent was used as the etchant. Microphotographs were made on several of the microstructures for futher optical and metallurgical investigations.

Test Results

Table 1 presents the list of tests conducted and the pertinent test parameters. Table 2 gives some of the threshold conditions for the titanium alloy. Figure 1 shows a full size one dimensional macrophotograph of the test specimen after it had been fractured by the final static tension load.

Figure 2 shows the emission data output over 55000 fatigue cycles at 30 Hz and a gain of 85 dB and bandpass filtered at 0.1 to 0.3 MHz taken from specimen 5. During this period no crack appeared on the surface of the specimen under test. The compliance load was checked occasionally and this compliance remained constant as can be seen in Figure 3. The first emission crack growth data is seen at about 92440 cycles as burst type signals accumulated for a one second interval on opening and closing of the crack then recorded as a log plot in counts per second. In Figure 4 crack output data if plotted only between the peak volts of 1.00 and 1.80 volts as a log plot in counts per second. Figure 5 presents acoustic signals of cyclic crack growth and also signals of crack growth in a non-cyclic period of minimum load approixamately 100 lb(444 N) extending over an eight minute period. The emission output data shown are representative crack growth data of the test specimens used in this investigation.

Figure 6 shows the specimen after the fatigue crack arrested and complete fracture was made. A very small amount of shear is seen at the surface edge of the crack,

indicating a plane strain condition prevailed during the fatigue cycle period of the test.

Figure 7 reveals the microstructure crack formation at 15 to 22 degree angles to the advancing crack during the fatigue cycle period. The microstructure from specimen 5 out of the section that was under a static tension load to fracture can be seen in Figure 8. This section contains intergranular and intragranular cracks moving somewhat perpendicular to the advancing fracture. This was not considered as part of the stress crack emission test.

Figure 10 presents the stress intensity factor (K) as a function of crack length in the titanium alloy tested (Ti6Al4V). Figure 11 shows a relationship of the stress intensity factor (K) to the crack growth rate.

Figure 12 presents the data on specimens 4 and 5 that show a relationship of the acoustic emission counts to crack growth. The WOL test specimens 1 and 2 were lost in the compliance calibration process and could not be used in the investigation.

Discussion of Results

The effect of the dry grade nitrogen gas (99.9%) on the titanium alloy grain structure while in the furnace during heat treating was not completely investigated. This area shall be examined more effectively as a part of the environmental aspects of the study.

Cracks were observed to grow in and along the grain boundaries in test specimen 5 , but this phenomenum was not observed in the other two tested specimens. While nitrogen gas does react at high temperatures to form excess nitrogen dioxide and tetroxide and these do increase the possibility of stress cracking in titanium alloy, this phenomenum is not considered as the condition here. The design and principle of the furnace are such that all moistures and other gases within the furnace box are burned off during the dry-out and purge period. Since this type microcracking was observed in only specimen 5, it is thought that this is a supporting reason to eliminate the nitrogen effect.

The surface of the specimens were cleaner and the titanium oxide film was thinner (0.001 in) and removed easier with silicon carbide abrasive wet/dry belt. As much as 0.006 in. of surface metal was removed from each side of the specimen to obtain the smooth surface for testing. This is a time consuming operation. The next titanium alloy shall be cut close to the actual size of the test specimen and heat treated, then machined to the actual specimen's specifications. This may improve the surface and reduce surface finishing time.

The specimens were placed in a tightly sealed decissicator for protection from the environment and were removed and marked only at the time of testing.

The load compliance (ΔP) was determined for each test specimen so that a plane strain condition was maintained. The MTS clip gage through the strain control module controlled the load compliance calibration for each specimen. A strain hardening effect was achieved at the loading pin to pin hole interface by the initial loading before the fatigue cycling and this was effective in eliminating excess noise from the pin and pin hole during the fatigue cycling. Specimens 1 and 2 were over stressed during the compliance calibration and a premature crack occurred at the cold worked notch tip. These were excluded in the investigation. Six WOL test specimens should be tested under uniform reproducable conditions in order to see the real time energy release to the crack growth rate and AE counts.

The acoustic emission counts were observed to be cyclic and also to occur in a non-cyclic period at minimum load in specimen 5. The magnitude of the acoustic signals under this condition decreased when compared to the signals in the cyclic period, Figure 4. That is, the emission rate continued for about 8 minutes at a minimum load (100 lb) and no fatigue cycles. This may suggest a strain hardening effect during the fatigue cycle that produces additional energy at the grain boundary interfaces. In Figure 4 the output data suggest that the strongest and highest concentration of emission seem to occur at the initial crack burst and decrease with time. In real time, the initial energy was in the order of magnitude 10^2 counts which lasted for a period of 30

seconds then decreased to zero emission in 20 seconds, followed by a very low output. During the next 10 seconds nothing occurred, then instaneously a high energy release of the order of magnitude 10^6 counts, and within the next 10 seconds the energy level was back at zero emission. It is in this type condition that information should be developed to show a correlation of the magnitude of real time crack growth, growth rate and energy release.

The crack growth rate was in the order of 10^{-2} to 10^{-6} inch per cycle and difficult to optically detect on the smooth surface of the titanium alloy, Table 2. No crack advancement was observed on the surface at this time period and this made it difficult to identify the area of concern in the microstructure without additional acoustic emission instrumentation. Further investigation should be directed at the development of additional data in this area.

The acoustic signals of the crack growth rate were an accumulation of counts in the opening and closing fatigue cycle, but the specimen was always in tension so the crack did not close. In Figure 2 the continuous linear acoustic emission recorded on specimen 5 are typical to that of specimens 3 and 4 during the first 40000 to 95000 fatigue cycles.
A linear plot of the emission counts over the fatigue life cycles on the test specimen was recorded by the x-y plotter. The acoustic emission system now in use was able to detect small and large crack growth. Much of the crack growth rate

detected by the AE system was not visible through our 32X traveling microscope, indicating that the crack growth rate in emission counts per time interval is more valid than crack growth rate per cycle. The final acoustic data output recorded from specimen 5 during the last four minutes of the fatigue period, Figure 13, is an example of crack emission signals; however, the visible crack on the surface did not extend.

The amplitude of the acoustic signals recorded in the opening fatigue cycles were of a higher order of magnitude than those in the closing fatigue cycles.

The AE output of the crack growth presented in Figure 13 on specimen 5 suggest that the subcritical stress intensity factor (K_{sc}) had not reached threshold level since there were the high concentration of emission at a gain of 85 dB after some 933490 cycles. However, the test was terminated and the specimen was statically loaded to complete fracture for microstructural examination.

The microstructure consist of transformed beta containing elongated platelike alpha (light) which occurred with the annealing process at 722 C(1350 F). The microcracks occurred intergranular in the beta structure, Figure 7. The small segements formed as the crack moved away from the main advancing branch and moved back into it. Figure 8 shows the crack formation below the main advancing crack during the

static loading of the test specimen to complete failure. These are perpendicular to the direction of the crack movement and the rolling direction of the metal.

The microstructure shown in Figure 9 is from a section that runs parallel to the rolling direction of the material and was cut approximately 0.250 in (6.35 mm) below the section shown in Figure 7. The microstructure is characteristic of the heat treated material used in this investigation and no cracks appeared in this section. The plate-like alpha (Widmanstatten) structure is revealed at the boundaries, with some surrounding alpha prime in the beta matrix. Further observations will be made in the following investigation on the performance of this specific type heated treated alloy.

Conclusions

The following conclusions are drawn from the test results obtained during the investigation:

1. The acoustic emission system provides a sensitive tool for detecting crack growth in the titanium alloy.
2. Crack growth rates of 10^{-6} in/cycle were dtected at 85 dB and 0.1 - 0.3 MHz.
3. The acoustic emission was consistently observed to be cyclic in nature.
4. The acoustic emission was observed during a few non-cycle low static load periods. This may be related to a strain hardening effect during the fatigue cycle.
5. A peak level in the acoustic emission count rate was observed in all the tests. There may be some relation here in the plane strain - plane stress transition at the instantaneous growth in the crack.
6. The effects of various test parameters on the threshold conditions in the crack growth detection can be seen in Table 2.
7. The high concentration of acoustic signals observed from specimen 5 when the crack appeared to have arrested by optical measurement may indicate that the subcritical stress intensity level (K_{sc}) was not reached.

Conclusions

8. Microcracks were observed below the advancing crack moving at angles other than parallel to it. The intergranular cracks were not considered as an effect of the nitrogen gas during heat treating.
9. The quantitative comparison of microcracks and crack extention to the exact energy release at that crack amplitude was not determined.
10. The solution heat treating produced an increase in the yield strength with some loss in ductility.

References

1. ASTM Standard Committee, A-24, Part 10, American Society for Testing Materials, Philadelphia, Pa., 1974.

2. ASTM Standards Part 10, E 399-75, American Society for Testing Materials, Philadelphia, Pa., 1975.

3. ASM Source Book on Heat Treating, Vol. 1, Materials and Processess, 1975, Metals Park, Ohio, pp. 254-367.

4. Titanium Metals Corporation of America, Properties of Ti6Al4V", Titanium Engineering Bulletin No. 1, 1965.

5. Harris, D.O. and Dunegan, H.L., "Continuous Monitoring of Fatigue Crack Growth By Acoustic Emission Techniques", Technical Report DE-73-2 Feb. 1973. Dunegan/Endevco, San Juan Capistrano, Calif.

6. Tatro, C.A., Liptai, R.G. and Moon, D.W., "Acoustic Emission From Formation and Advancement of Cracks", March 5, 1973, UCRL-74607, Lawrence livermore Lab., Livermore, Calif.

7. Harris, D.O., "The Effect of Gain and Frequency Bandpass on Acoustic Emission Observed From Growing Fatigue Cracks", Jan. 1974, Dunegan/ Endevco, San Juan Capistrano, Calif.

Problems

A major effort in this investigation was to be directed at cyclic fatigue and environmental stress cracking using the acoustic emission technique to obtain data that could be correlated to show a relation between the crack growth rate and the magnitude of the released energy amplitude signals. This data was not obtained since the necessary additional AE instrumentation did not arrive early enough for application during this period. Time became a factor for making some accomplishment during the investigation period. Unfortunately, communications were slow and at times seemed to have come to a halt. This resulted in my budget officer delaying approval for the purchase of the accessory AE instrumentation such that these could be used effectively in this investigation period. We finally recieved an approval letter dated May 5, 1980.

Application of the aboved mentioned instrumentation shall be made during the next period of investigation on this problem. The energy processor, one of the AE instruments has not yet arrived, but the purchase was approved.

Appendix

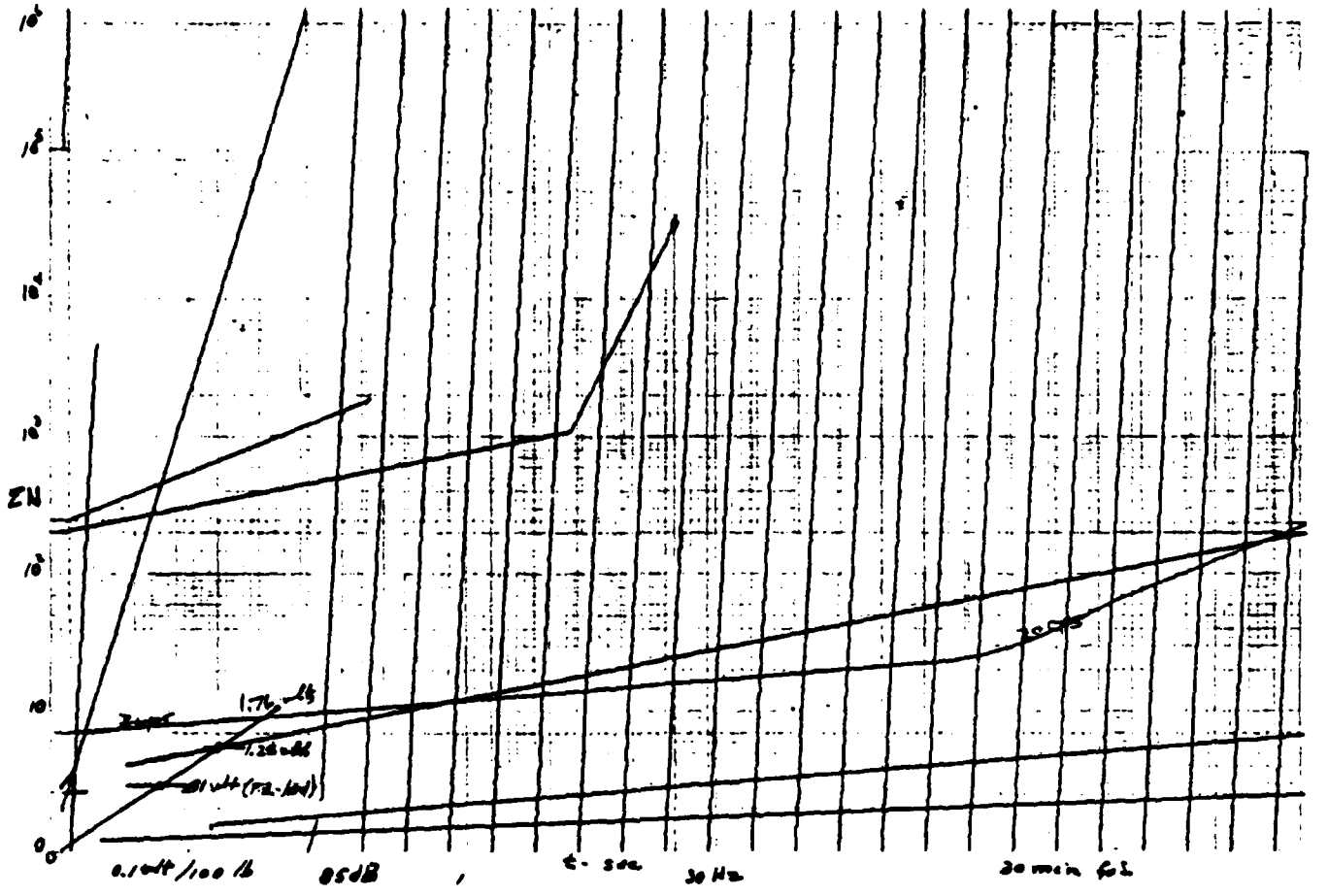

Figure 2. Acoustic emission output at 85 dB and 0.1 -0.3 MHz over 93400 cycles at 30 Hz. The compliance calibration is shown at the lower left. Data taken from specimen 5.

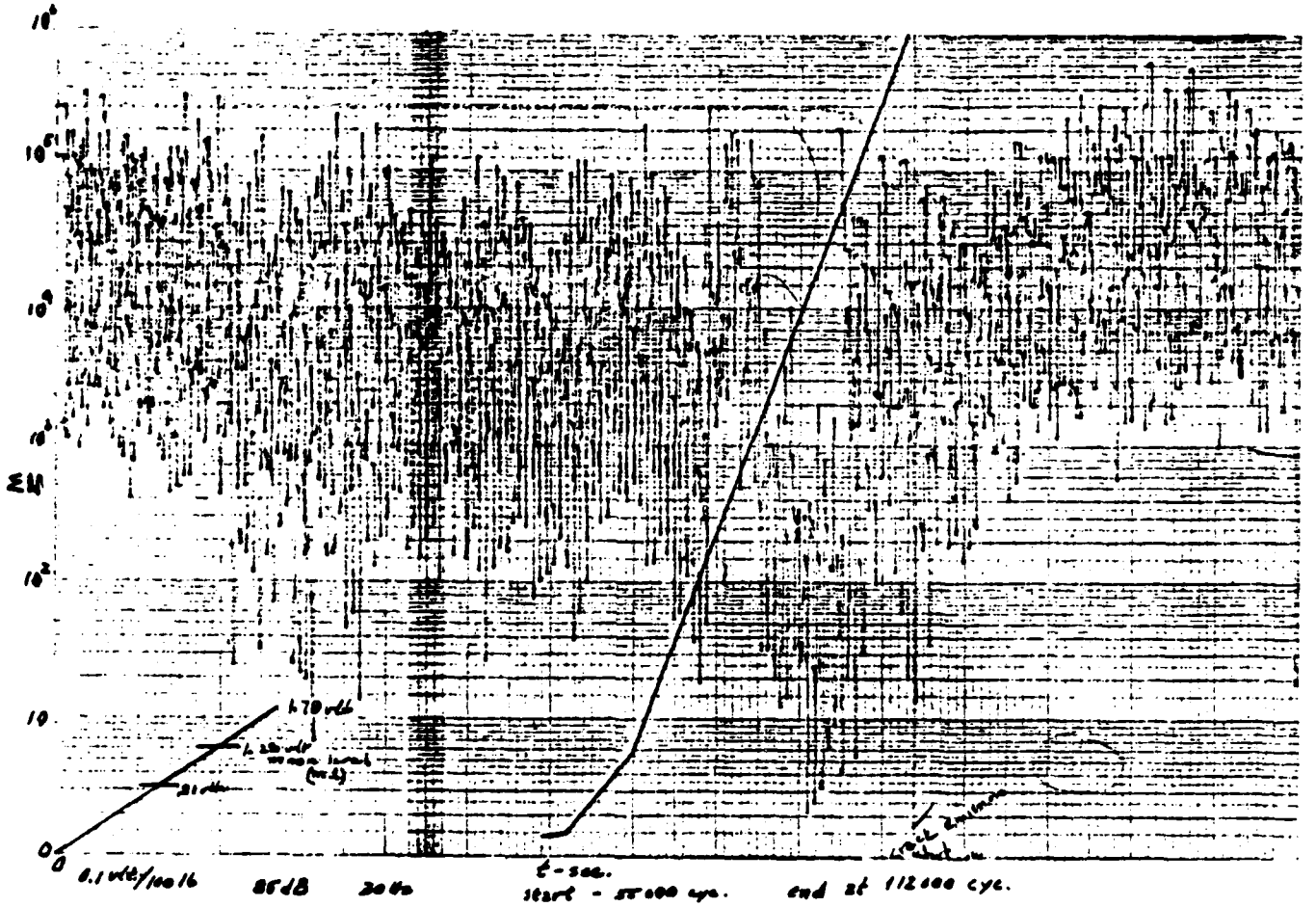

Figure 3. This represents the acoustic emission output in real time at the starting of the crack growth in the last eighteen minutes of the full scale. 85 db, 0.1 - 0.3 MHz and 30 Hz range, specimen 5. The heavy black line shows the last acoustic signal before the crack growth bursts were observed.

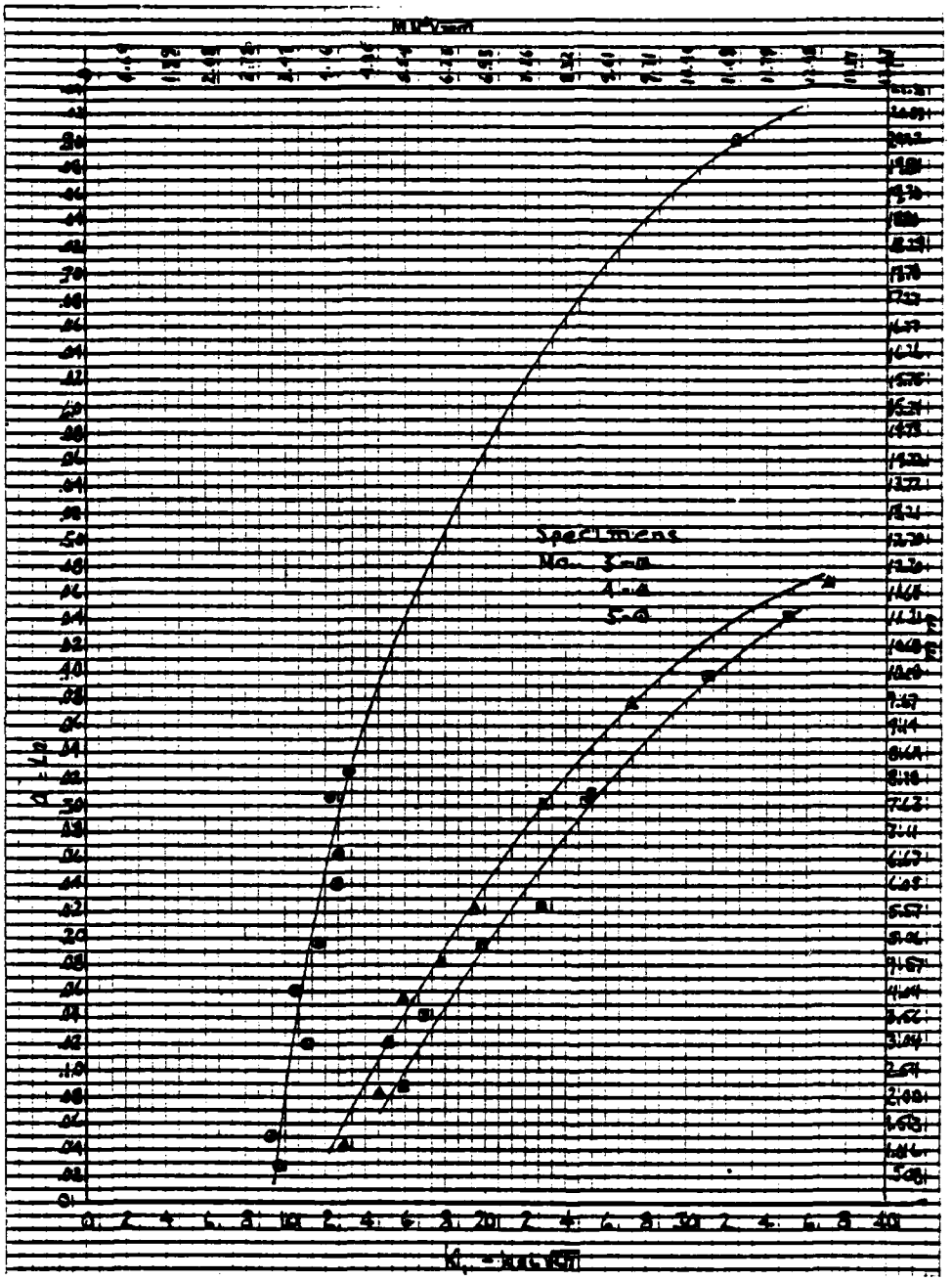

Figure 10. A linear relationship between the crack growth rate and the stress intensity factor (K_1).

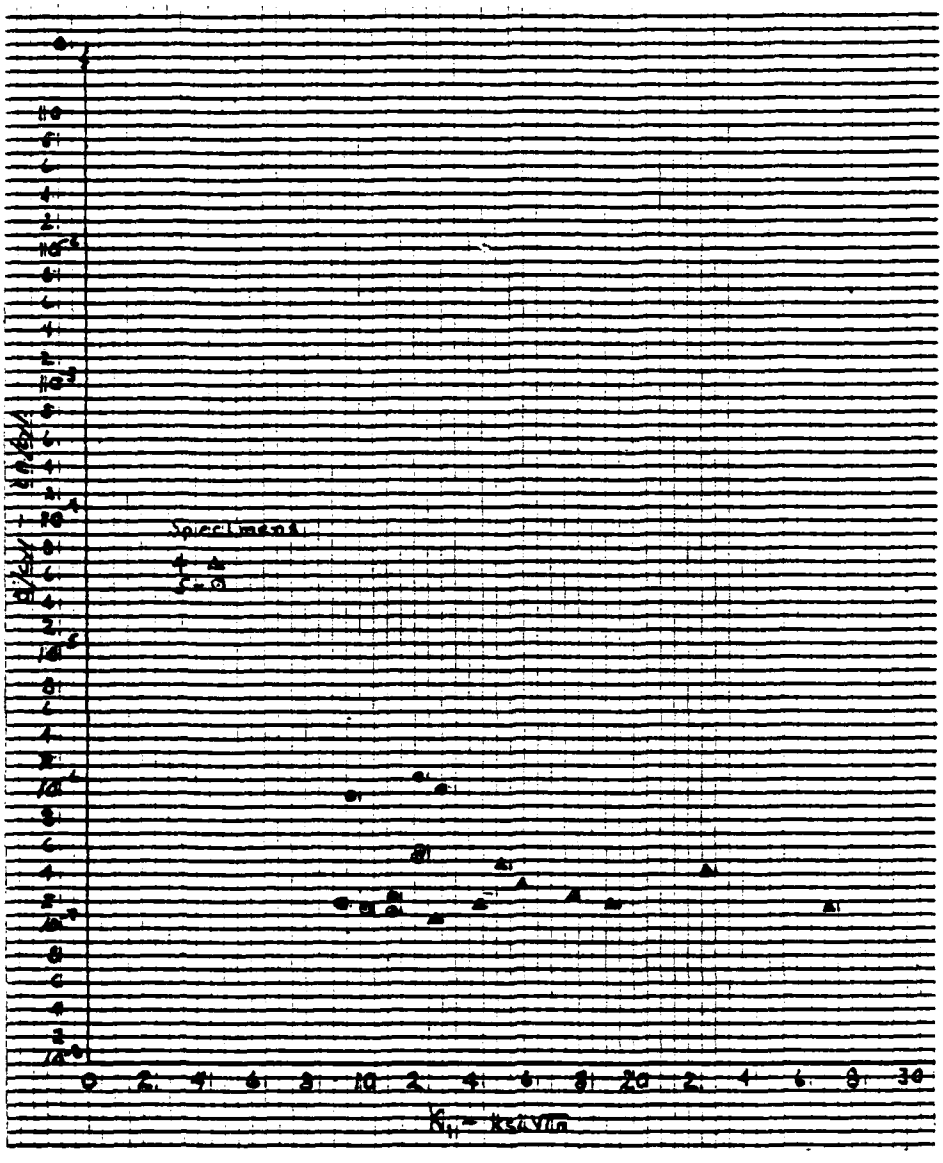

Figure 11. The spread in the crack growth rate versus stress intensity (K_I) is too large in specimens 4 and 5 for any specific predictions.

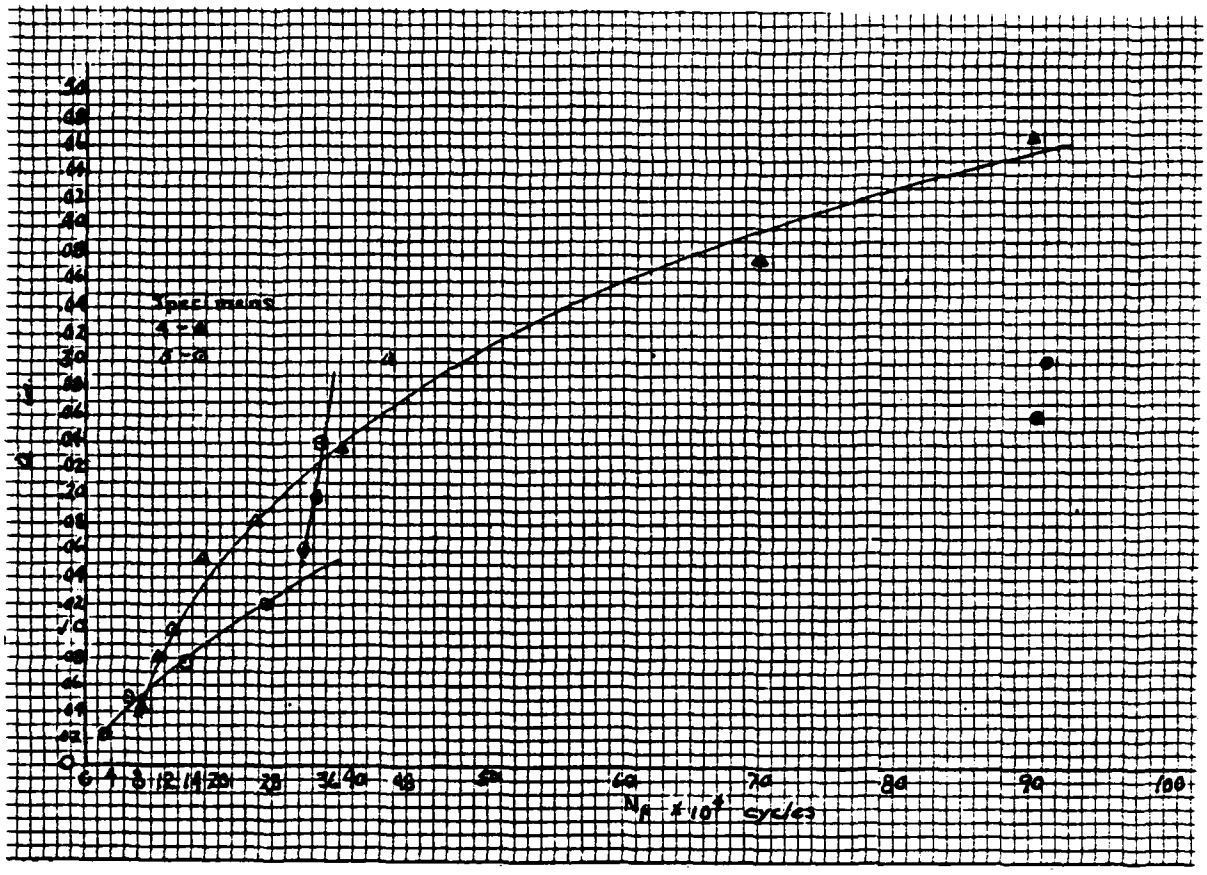

Figure 12. The non-linear curve shows a relationship of the crack growth versus the total number of fatigue cycles for that crack in the heat treated specimens (Ti6Al4V).

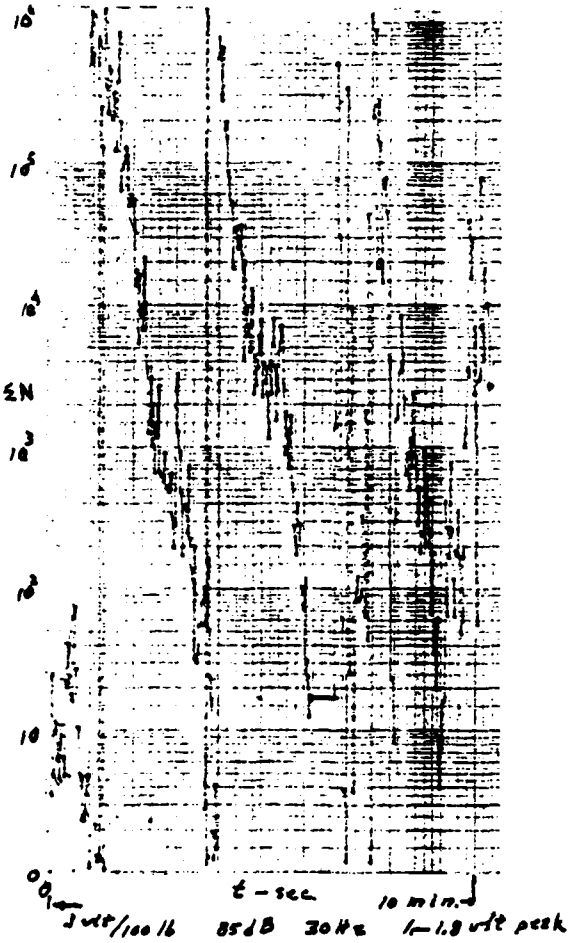

Figure 4. The summation of acoustic emission counts to real time crack growth at 85dB and 30 Hz recorded between 1.0 - 1.80 volts over a 10 minute interval.

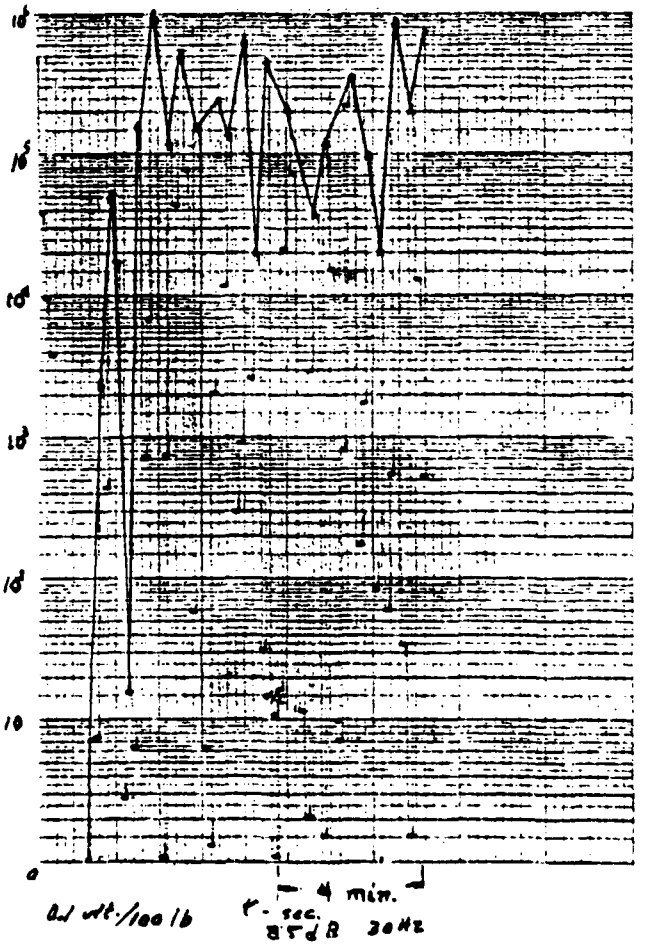

Figure 5. A summation of AE counts to crack growth rate at a 2 seconds reset clock interval. A 4 minute period of AE signals during no cycle and a minimum load (ΔP) was observed.

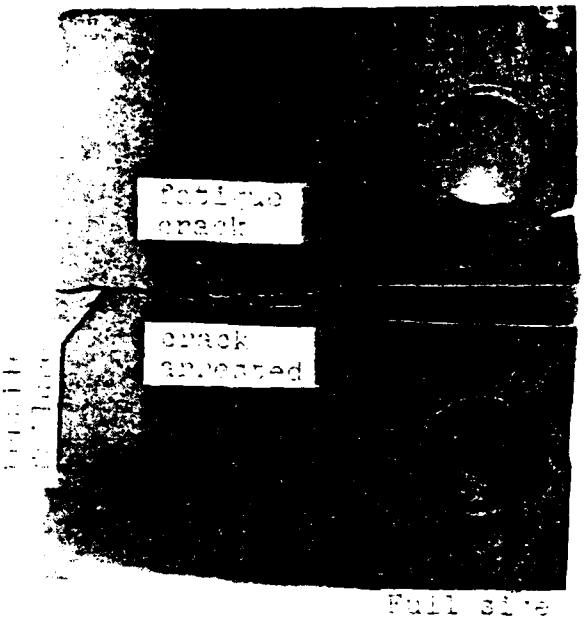

Figure 1. The 12.8 mm (0.510 in) WOL compact test specimen reveals the fatigue crack growth length. The small pads on the edge held the clip gage.

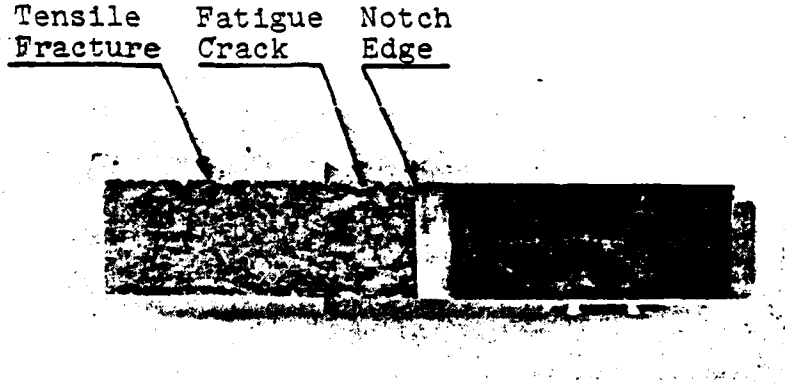

Figure 6. The WOL compact specimen shows the fatigue structure (actual size).

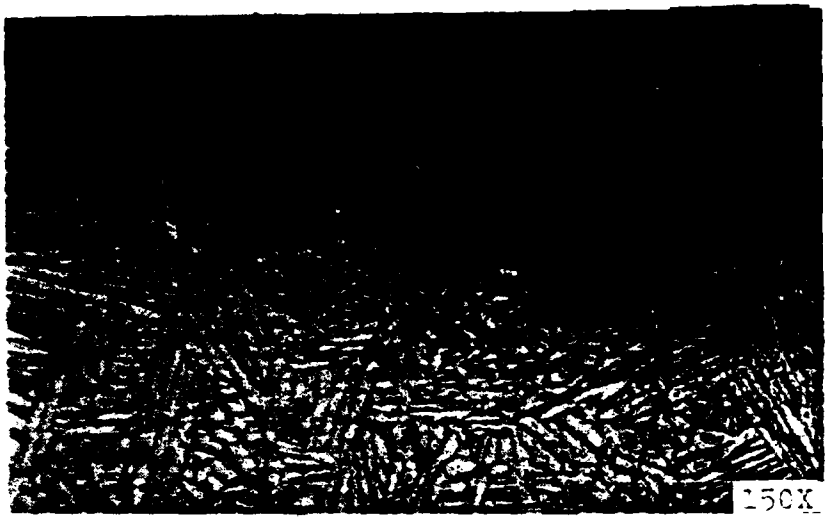

Figure 7. Coarse platelike alpha microstructure with the microcracks growing at an angle ≈15 degrees to the advancing fatigue crack in the heat treated specimen.

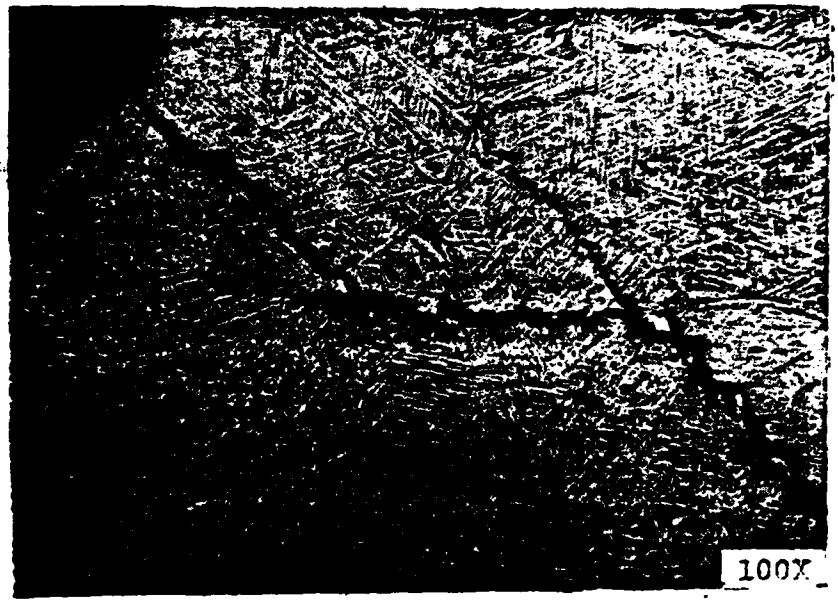

Figure 8. The microphotograph shows intergranular microcracks in the transformed beta of the titanium alloy.

Figure 9. The microphotograph shows coarse platelike alpha (light) and transformed beta found in the heat treated titanium alloy.

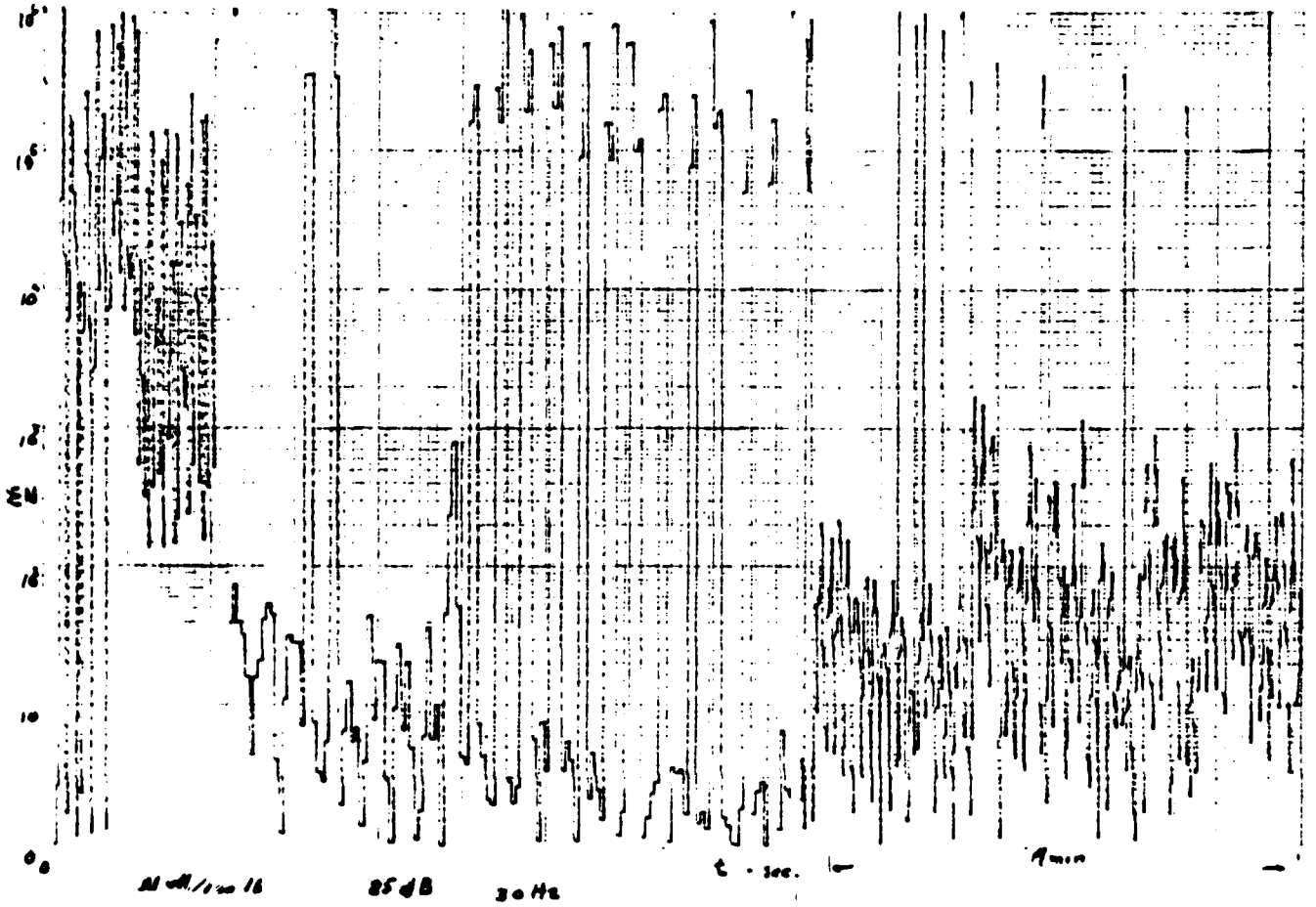

Figure 13. The high concentration of acoustic emission is seen near the end of the proposed fatigue cycle period. Over 933490 fatigue cyles completed. The crack showed no optically measurable growth through the traveling microscope.

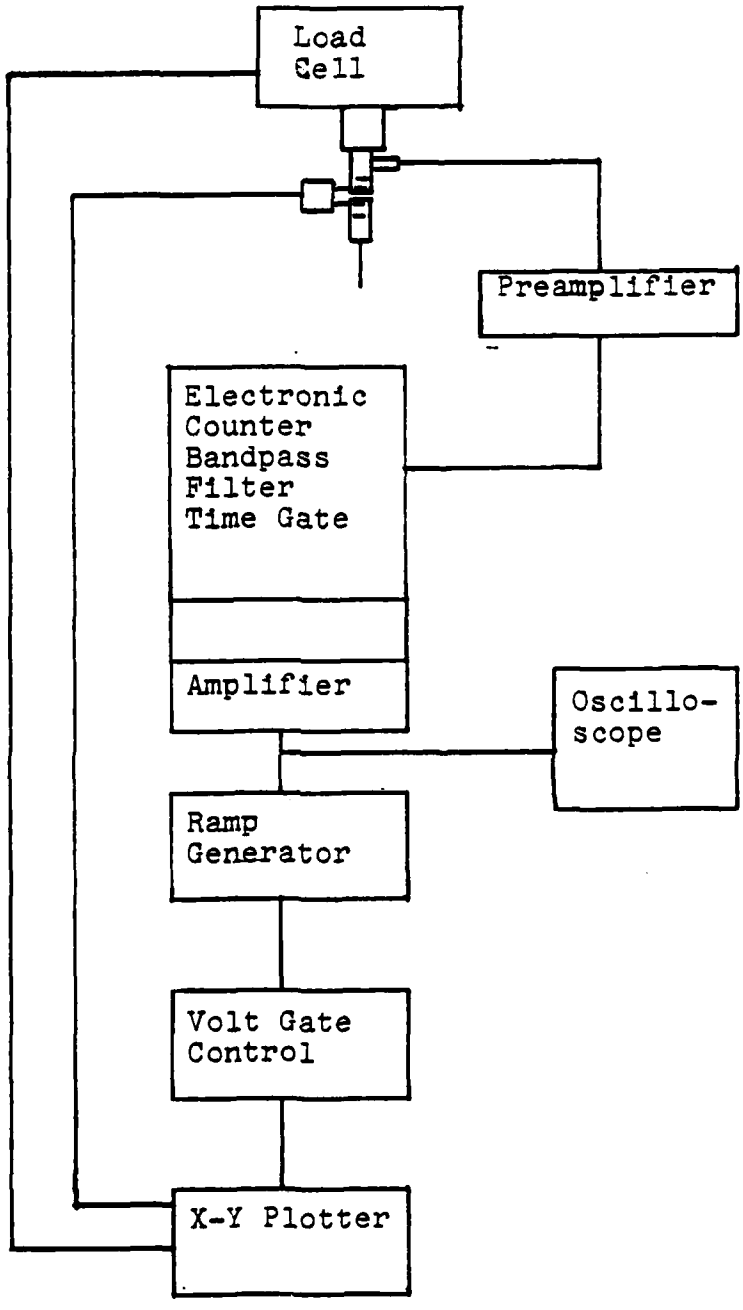

Figure 14. A block diagram of the test instrumentation.

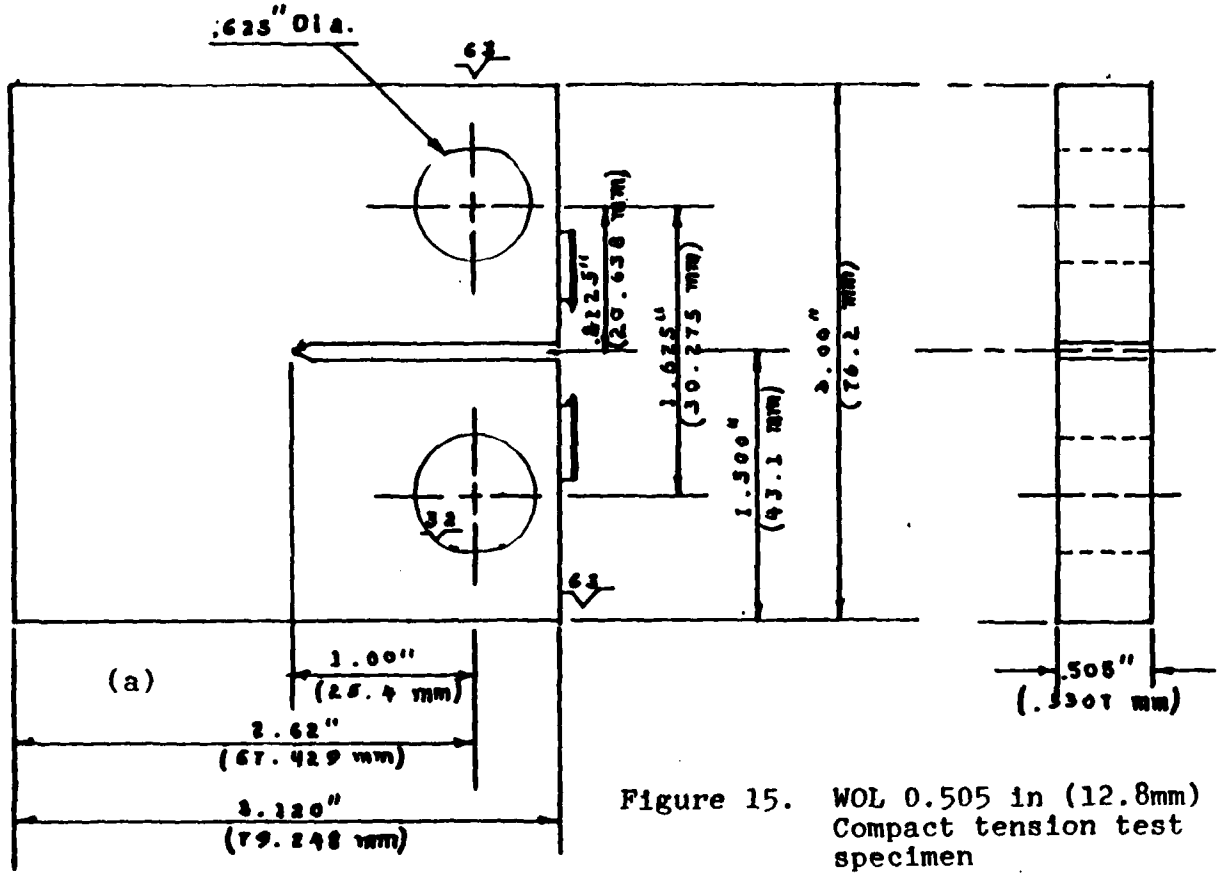

Figure 15. WOL 0.505 in (12.8mm) Compact tension test specimen

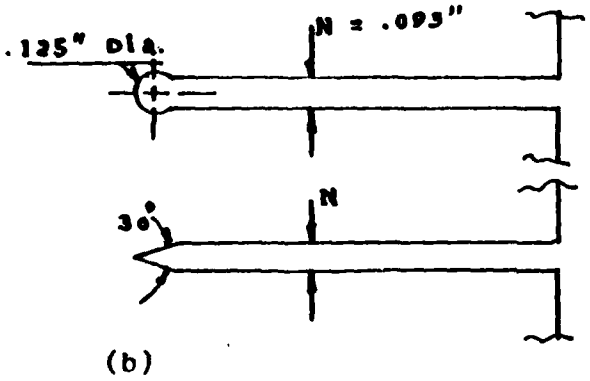

SOUTHERN UNIVERSITY
Mech. Engr. Dept.
Baton Rouge, Louisiana

Compact tension Specimen
(COD) Close-open-Displacement

Drawn by: Scale: 1"=1"

Approved by: Date:

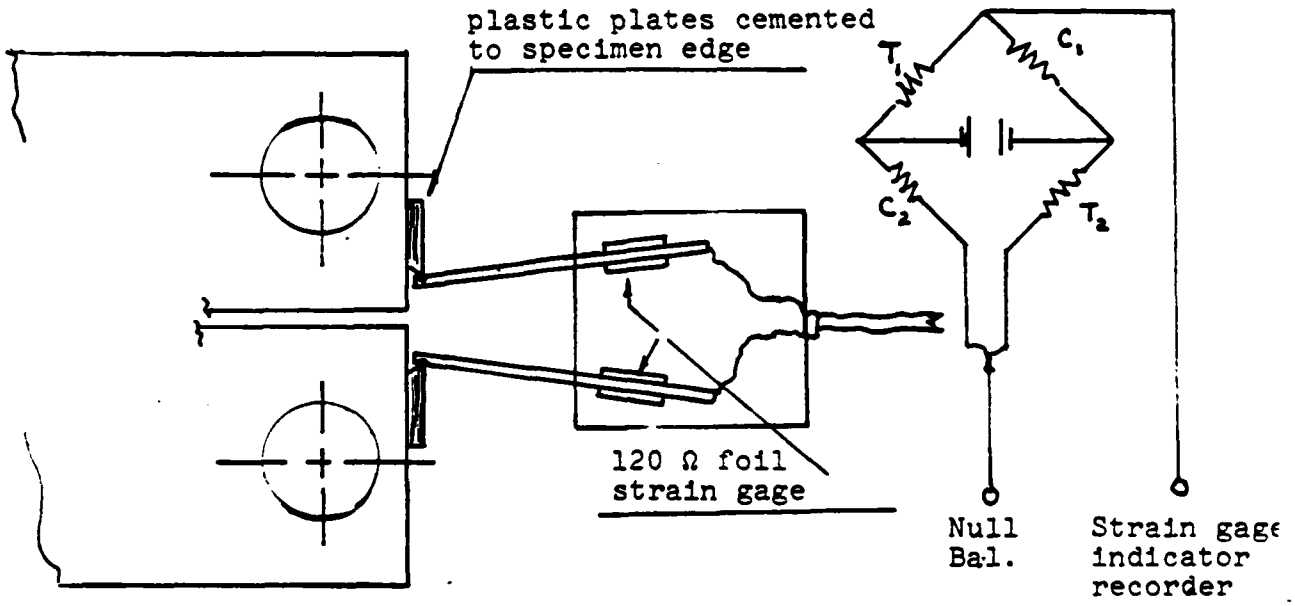

Figure 16. Double cantilever beam strain gage and method of mounting on specimen and measuring displacement; thus load compliance.
The method of employing electric resistance strain gages mounted on a suitably designed flexural element to measure the notch opening under a designed load has been used by other experimenters.

Table 1. Test parameters related to the acoustic emission detection in the titanium alloy (Ti6Al4V).

Specimen 5 a(in)	(mm)	cyl(30Hz)	Specimen 4 a(in)	(mm)	cyl(30Hz)
.027	.701	27930	.043	1.09	85230
.0239	.608	14120	.082	2.08	23590
.069	1.758	29700	.102	2.60	21220
.040	1.006	32700	.154	3.91	47360
.037	.938	31303	.182	4.62	79800
.0456	1.158	7800	.234	5.95	122800
.020	.502	1500	.302	7.67	73800
.044	1.121	7730	.377	9.58	246203
.019	.479	1750			

Table 2. Threshold conditions for detecting acoustic emission in titanium alloy (Ti6Al4V).

Specimen 5 a/cyl x 10^{-6}	Ksi$\sqrt{in}$	$MN^2\sqrt{mm}$ x 10^{-4}	Specimen 4 a/cyl x 10^{-6}	Ksi$\sqrt{in}$	$MN^2\sqrt{mm}$ x 10^{-4}
9.70	9.52	3.40	0.50	12.73	4.42
1.70	9.25	3.21	1.80	14.39	4.99
2.30	11.00	3.82	4.80	15.15	5.25
1.20	10.15	3.52	3.30	15.96	5.53
1.18	11.43	3.96	2.30	17.72	6.15
5.90	12.14	4.20	1.90	19.31	6.70
13.	12.80	4.23	4.10	22.61	7.84
5.7	12.07	4.18	1.50	27.33	9.48
11.	12.89	4.47			


DATE
ILME